JOURNAL OF APPLIED PHYSICS **115**, 043522 (2014)

Temperature recovery from degenerated infrared image based on the principle for temperature measurement using infrared sensor

Zhiyuan Zou,[1] Yihua Hu,[1,a)] Bin Gao,[2,3] W. L. Woo,[3] and Xinyu Zhao[1]
[1]*College of Electrical Engineering, Zhejiang University, Hangzhou, China*
[2]*School of Automation Engineering, University of Electronic Science and Technology, Chengdu, China*
[3]*School of Electrical and Electronic Engineering, Newcastle University, England, United Kingdom*

(Received 15 November 2013; accepted 19 January 2014; published online 30 January 2014)

Thermal camera has been applied in photovoltaic (PV) array monitoring to detect defects and hot spots. However, the infrared (IR) image is often degenerated and the temperature information displayed from the image can lead to erroneous interpretation. Hot spots will be obscured and a gradual change phenomenon will emerge when monitoring a large PV array. In this paper, the mechanism of IR image degeneration and gradual change phenomenon are studied and verified with experiments. The variations of atmospheric transmission and directional emissivity have been identified to be the cause of image degeneration. The sensitivity of atmospheric transmission and directional emissivity are defined to analyze the impact of these two factors on the temperature displayed. Based on this mechanism, a recovery method has been proposed to recover the real temperature from the degenerated IR image. Experiments have been conducted to test the effectiveness of the recovery method. In addition, the temperature sensitivity has been defined to analyze how atmospheric transmission and directional emissivity will affect the temperature difference displayed in the IR image. The proposed temperature sensitivity has been used as the criteria to assess the quality of IR image. Some rules of thumb are proposed to deploy the thermal camera in order to increase the quality of the IR image.
[http://dx.doi.org/10.1063/1.4863783]

I. INTRODUCTION

Thermal camera has been applied in photovoltaic (PV) array monitoring to detect defects. When a defect exists in the PV module, the temperature becomes distinguishably high. Modern thermal camera can detect the temperature of the PV module and displays it in the infrared (IR) image. Thermal camera used for detecting defects brings advantages such as easy to use and non-contact requirements, which has made topic to be an active research. A lot of effort has been invested to study the correctness and preciseness of this method, yet not much emphasis has been paid to the quality of the IR image itself. However, the temperature displayed in the IR image is often incorrect and will lead to misleading conclusions. IR image taken at different distance or at different angles can yield varying results. In addition, when monitoring a large PV array, a gradual change phenomenon will emerge (see Fig. 1): PV modules at further distance appear to be cooler than PV modules at close distance. Defects at further distance can be obscured. This phenomenon has yet to be researched. In previous study about the PV module monitoring, the unrecovered temperature displayed in the IR image has been used as the temperature of the PV module, which can be erroneous.[1–21]

In this paper, the cause of the IR image degeneration has been identified. A method has been proposed to recover the actual temperature of the degenerated IR image. The major contributions of this paper are

(1) Identify the cause of IR image degeneration and propose a method a recover the real temperature from the degenerated image.
(2) Define atmospheric transmission sensitivity and directional emissivity sensitivity to evaluate how the two factors can affect the temperature displayed from the IR image.
(3) Define temperature sensitivity as the criteria to assess the quality of the IR image and give some rules of thumb to increase the image quality when taking IR image.

The structure of this paper is as follows: Sec. II introduces the principle of temperature measurement using infrared camera. Section III focuses on the two main factors leading to the gradual change phenomenon, namely, the variation of atmospheric transmission and directional emissivity. Section IV discusses the effect of ambient factors on the experiment results. Section V illustrates the equipment for the two experiments. Section VI records and analyzes the results of experiments for directional emissivity measurement. Section VII records and analyzes the results of experiments for atmospheric transmission measurement. Section VIII illustrates the method of temperature recovery and the experiment to test this method. In Sec. IX, the atmospheric transmission sensitivity and directional emissivity sensitivity have been defined to analyze the impact of these two factors on the temperature displayed. Concurrently, temperature sensitivity has been defined to analyze whether the real temperature difference will be obscured in the IR image. Section X presents the rules of thumb and restrictions about the position of thermal camera. Final conclusion is drawn in Sec. XI.

a)Author to whom correspondence should be addressed. Electronic mail: huyihuacumt@126.com

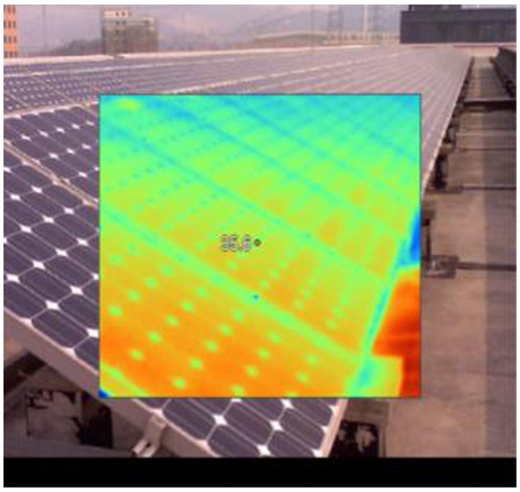

FIG. 1. Gradual change phenomenon in IR image of large PV array.

II. THE PRINCIPLE OF TEMPERATURE MEASUREMENT USING INFRARED CAMERA

In order to study the cause of gradual change phenomenon, it is necessary to understand the principle of infrared temperature measurement, which will be explained in Secs. II A and II B.

A. Black body, grey body, and selective absorber

A black body is an idealized physical body that absorbs all incident electromagnetic radiation and emits the same amount of electromagnetic radiation in thermal equilibrium, regardless of frequency or angle of incidence. According to the Stefan–Boltzmann law,[23] the total energy radiated per unit surface area of a black body across all wavelengths per unit time (also known as the black-body radiant existence or emissive power) $M_b(T)$, is directly proportional to the fourth power of the black body's thermodynamic temperature T, as indicated in Eq. (1)

$$M_b(T) = \sigma T^4. \tag{1}$$

A grey body is a body that does not absorb all incident electromagnetic radiation but the amount of electromagnetic radiation absorbed is proportional to that of the black body, regardless of frequency. The proportion between the emitted energy of a grey body and a black body of the same thermodynamic temperature T can be characterized as emissivity ε.

A selective absorber is also a body that does not absorb all incident electromagnetic radiation. The difference between a selective absorber and a grey body is that the proportion between the emitted energy of a selective absorber and that of a black body of the same thermodynamic temperature T is not a constant but a variable dependent on the frequency λ. The difference can be demonstrated as follows:

For a selective absorber: $\varepsilon_{\lambda 1} \neq \varepsilon_{\lambda 2}$.
For a grey body: $\varepsilon_{\lambda 1} = \varepsilon_{\lambda 2}$.

The relationship between these objects is illustrated in Fig. 2.

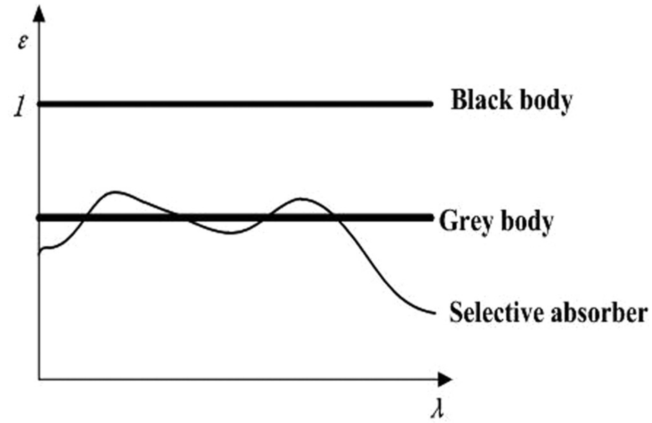

FIG. 2. Black body, grey body, and selective absorber.

B. Temperature measurement using infrared camera based on a grey body approximation

Inagaki and Yoshizo[23] have developed a theory of temperature measurement and studied the various properties of different infrared sensors that work in different bands. According to Inagaki's work, the method of temperature measurement requires two pre-requisites: (1) The object is in thermal equilibrium and (2) a grey body approximation can be applied. Although most objects in real life are not grey bodies, in the bands which infrared sensors work the emissivity is usually relatively independent of the frequency, and thus, the grey body approximation can be applied. Based on the two pre-requisites, the theory of temperature measurement using infrared camera can be illustrated as follows.

The irradiance received by the camera consists of three parts, the irradiance emitted and reflected by the surface, and the irradiance emitted by the atmosphere, as demonstrated in Fig. 3. The atmosphere absorbs part of the irradiance from the detected surface and emits irradiance at the same time. As the distance increases, the percentage of atmospheric irradiance in the total received irradiance becomes larger.

For the infrared camera, the total received irradiance equals to[23]

$$I(T_R) = \tau_a\left[\varepsilon I(T_0) + (1-\alpha)I(T_u)\right] + (1-\tau_a)I(T_a), \tag{2}$$

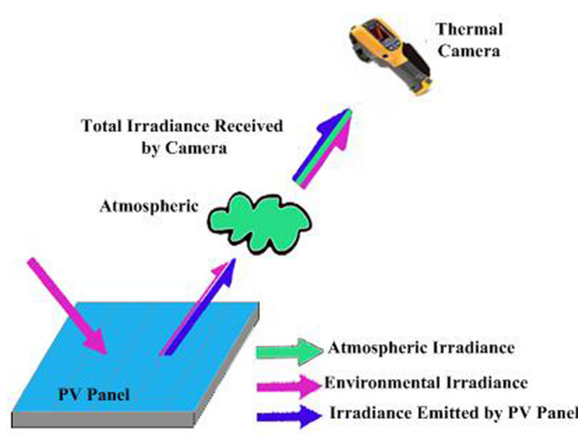

FIG. 3. Irradiance received by infrared camera.

where $I(T_R)$ is the total irradiance received by the camera, $\varepsilon I(T_0)$ represents the irradiance emitted by the PV panel, $(1-\alpha)I(T_u)$ stands for the environmental irradiance reflected by the PV panel, and $I(T_a)$ denotes the irradiance emitted by the atmosphere. The term τ_a denotes the atmospheric transmission which ranges from 0 to 1. T_0 represents the real temperature and T_R represents the displayed temperature of the infrared camera. T_u denotes the temperature of the environment and T_a is the temperature of the atmosphere. Note that in this paper, all temperature used for calculation is given in Kelvin temperature. The irradiance of an object with a temperature T can be calculated as follows:

$$I_R(T) = CT^n, \tag{3}$$

where C is a constant. Most infrared cameras work within the infrared spectral bands of either $2\sim5\,\mu$m or $8\sim13\mu$m. For $2\sim5\,\mu$m, $n=9.2554$; for $8\sim13\,\mu$m, $n=3.9889$.

Equation (2) can be rewritten as follows:[23]

$$T_R^n = \tau_a\left[\varepsilon T_0^n + (1-\alpha)T_u^n\right] + (1-\tau_a)T_a^n. \tag{4}$$

Because the measured object is approximated as a grey body, the following equation exists:

$$\varepsilon = \alpha. \tag{5}$$

The infrared camera used in this paper works in the band of 7.5 μm to 14 μm, thus n $\approx$ 4.

Equation (4) can be rewritten as

$$T_R^4 = \tau_a\left[\varepsilon T_0^4 + (1-\varepsilon)T_u^4\right] + (1-\tau_a)T_a^4. \tag{6}$$

Equation (6) is widely applied in temperature calculation in infrared cameras. According to the theory of temperature measurement, two main impact factors responsible for the gradual change phenomenon in the IR image of PV array are the variation of directional emissivity and atmospheric transmission.[23] Other external factors will also affect the correctness of temperature measurement. In order to minimize the effect of these factors, a custom-made testbox has been used in the experiments, which is introduced in Sec. V.

III. TWO MAIN FACTORS LEADING TO THE GRADUAL CHANGE PHENOMENON IN IR IMAGE

A. The variation of atmospheric transmission

According to Eq. (6), the thermal signal received by the infrared camera consists of two parts, the thermal signal of the detected object (including the radiation emitted and reflected), and the thermal signal of the atmosphere. As the distance increases, the atmospheric transmission decreases; thus, the infrared camera receives less thermal signal from the detected object and more from the atmosphere, as displayed in Fig. 4, where

$$I(T_{R0}) = \varepsilon T_0^4 + (1-\varepsilon)T_u^4, \tag{7}$$

$$I(T_a) = T_a^4, \tag{8}$$

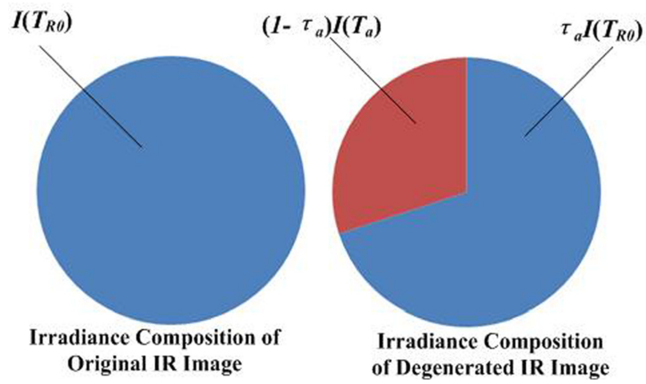

FIG. 4. Contrast between the irradiance composition of original and degenerated IR image.

where $I(T_{R0})$ represents the irradiance from the surface of the detected object, and T_{R0} is the displayed temperature when $\tau_a = 1$.

In the case of PV array monitoring, the temperature of the PV array surface is often higher than the temperature of the atmosphere. As the distance increases, the temperature detected by the infrared camera decreases because more irradiance is received from the atmosphere (see Eq. (7)). Therefore, PV modules at further distance appear to be cooler than PV modules at closer distance in the IR image.

In the case of PV array monitoring, the temperature of the PV array surface is often higher than the temperature of the atmosphere. As the distance increases, the temperature detected by the infrared camera decreases because more irradiance is received from the atmosphere (see Eq. (7)). Therefore, PV modules at further distance appear to be cooler than PV modules at closer distance in the IR image.

When monitoring a PV array of large area, the distance between the infrared camera and different parts of the PV array is different; thus, the atmospheric transmission is different, as presented in Fig. 5, where

$$I(T_{R1}) = \tau_1 I(T_{R0}) + (1-\tau_1)I(T_a), \tag{9}$$

$$I(T_{R2}) = \tau_2 I(T_{R0}) + (1-\tau_2)I(T_a). \tag{10}$$

Although the original irradiance from different parts of the PV array is the same ($I(T_{R0})$), the irradiance received by the infrared camera is different. Therefore, the displayed temperature of different part of the PV array in the IR image is different (see Fig. 1). In addition, even if the PV module is

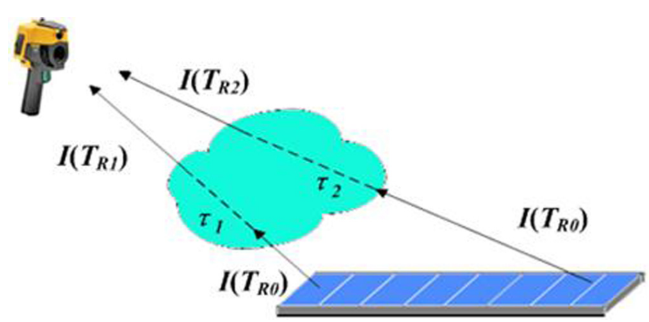

FIG. 5. Variation of atmospheric transmission when monitoring large PV array.

small and no gradual change phenomenon happens, the temperature from the IR image is still incorrect. This is because the camera calculates the temperature using $\tau_a = 1$ but in fact $\tau_a < 1$.

To test the impact of this main factor, experiments have been conducted; the results and analysis are illustrated in detail in Sec. VII. The quantitative analysis of this main factor is given in Sec. VIII.

B. Variation of directional emissivity

Besides the variation of atmospheric transmission, the other main factor leading to the degeneration of IR image and the gradual change phenomenon is the variation of directional emissivity.

1. Directional emissivity

The directional emissivity $\varepsilon(\theta)$ of an object is the emissivity measured from a certain perceived angle θ, as shown in Fig. 6. If an object has the characteristic that for any angles θ_1 and θ_2, $\varepsilon(\theta_1) = \varepsilon(\theta_2)$, such an object is called a lambert body. However, most objects are not lambert bodies, which means the directional emissivity is not a constant. According to the work of Schmidt and Eckert,[24] the emissivity of many non-metal objects remains constant when $\theta < 60°$; when $\theta > 60°$, the emissivity decreases quickly and ends up as zero. This is the reason the instruction of manual based infrared camera usually asks the user to hold the camera perpendicular to the detected surface and retain θ as zero. However, this is not practical when monitoring a large area of PV array, otherwise a large number of infrared cameras will be required. A more practical way to monitor a large PV array is to place the infrared camera at a certain location, which is exactly the method used in Fig. 1. As a result, the variation of directional emissivity can lead to the gradual change phenomenon in the IR image.

2. The impact of directional emissivity variation

In the case of PV array monitoring, the infrared camera is placed at a certain location; thus, the perceived angles between different PV panels are not constant but dependent on the distance between the PV panels and the infrared camera, as shown in Figure 7. As a result, PV panels at further distance emit radiation at a larger angle θ_2. If the PV panel is a lambert body, such a difference in the angle is not a

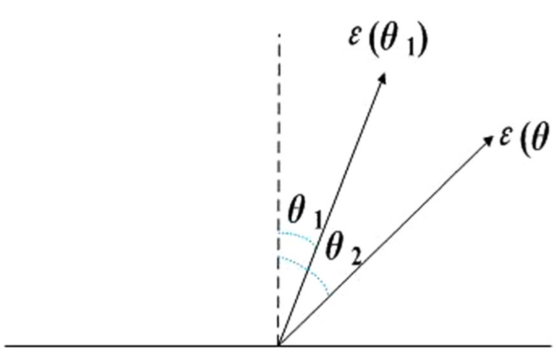

FIG. 6. Directional emissivity.

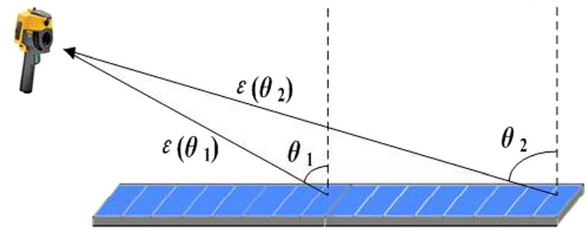

FIG. 7. Variation of directional emissivity when monitoring PV array.

problem. However, if PV panels have emission characteristics like the other non-metal materials indicated in the work of Schmidt and Eckert,[24] it is likely that $\varepsilon(\theta_1) > \varepsilon(\theta_2)$. According to Eq. (6), and the fact that $T_0 > T_u$, the difference between $\varepsilon(\theta_1)$ and $\varepsilon(\theta_2)$ can lead to the result that the detected temperature of PV panels from closer distance is higher than that of further distance. In addition, even if the PV module is small and no gradual change phenomenon happens, the temperature from the IR image is still incorrect. This is because the camera calculates the temperature using $\varepsilon(\theta) = 1$ but in fact $\varepsilon(\theta) < 1$.

Whether the difference of the perceived angle affects the result and quality of IR image depends on the characteristic of the PV panel's directional emissivity, which has not been studied or tested before. To learn the impact of this main factor, experiments have been conducted, which will be illustrated in detail in Sec. VI. The quantitative analysis of this main factor is given in Sec. VIII.

IV. AMBIENT FACTORS IN EXPERIMENTS—ENVIRONMENTAL TEMPERATURE, SUNLIGHT, AND WIND SPEED

The prerequisite of temperature measurement using infrared sensor is that the object must be in thermal equilibrium, which requires the environmental temperature to be relatively stable when performing experiments. Besides the environmental temperature, variation of the intensity of sunlight and wind speed can also break the state of thermal equilibrium. The fluctuation of the intensity of sunlight can lead to the difference of energy absorbed by the PV panel, thus result in the shift of temperature. The wind speed also has an influence to the result of temperature measurement using infrared sensor. According to the work of Jones and Underwood,[22] the following equation is derived to describe the heat loss of PV panel through convection:

$$q_{vec} = -(h_{c,forced} + h_{c,free}) \cdot A \cdot (T_{module} - T_{ambient}), \quad (11)$$

where q_{vec} represents the heat loss through convection, while A, T_{module}, and $T_{ambient}$ denote the area of PV module, the temperature of PV module, and the temperature of the environment, respectively. $h_{c,forced} + h_{c,free}$ is the coefficient that describes the physical condition of convection, which is strongly affected by the wind speed.

The forgoing three factors, namely, environmental temperature, sunlight, and wind speed, are of significant influence to the result of PV module monitoring. The quantitative description of the effect of such factors is not the focus of

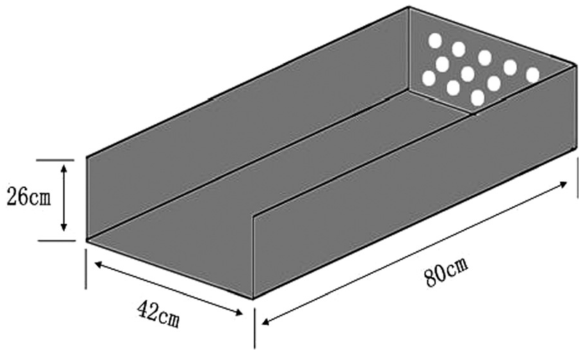

FIG. 8. Custom-made test box.

this paper, since the goal of this paper is to study the cause of the gradual change in IR image. The main focus is on the quantitative description of the two main factors proposed in Sec. III. The three environmental factors are stated to emphasize the importance of controlling them when performing outdoor experiments. In order to control these factors, a custom-made test box has been designed, which is illustrated in Sec. V.

V. EXPERIMENTAL SETUP

A. Custom-made test box

To minimize the effect of wind speed, variation of sunlight, and environmental temperature fluctuation, a custom-made test box made of translucent plastic is utilized, as shown in Fig. 8. The test box features a length of 80 cm and a width of 42 cm. The box is made small to ensure that the sunlight casted on the box remains relatively stable. Three sides of the box are surrounded by plastic walls, which have high heat capacity to maintain a relatively stable ambient temperature. The other side of the box is left open with no plastic wall so the infrared camera can monitor the PV module through this side. The opposite wall to the open side is drilled with holes to control the wind speed applied on the PV modules. A fan can be placed by the drilled wall to apply arbitrary wind speed, or a plank can be used to seal the holes to eliminate the effect of the wind.

B. Fluke Ti10 hardware and Smart View 3.1 software

In the experiment, a Fluke Ti10 infrared camera has been used for taking IR images. The parameter of the infrared camera is displayed in Table I.

The Smart View 3.1 software is used to process the IR images and mark out the temperature from the images.

TABLE I. Parameters of Fluke Ti10.

Parameters	Value
Accuracy	±5%
Detector type	160 × 120 focal plane array, uncooled micro bolometer
Infrared spectral band	7.5 μm to 14 μm
Field of view	23° × 17°

TABLE II. Parameter of PV modules.

Parameters	Value
Open voltage/V	4.8
Short current/A	0.23
MPP current/A	0.21
MPP voltage/V	3.85
Current temperature coefficient/°C	0.06%/K
Voltage temperature coefficient/°C	−0.36%/K
Power temperature coefficient/°C	−0.45%/K
Maximum power/W	0.8

C. PV module parameters

The parameters of the PV modules used in the experiments are listed in Table II.

VI. EXPERIMENTS OF DIRECTIONAL EMISSIVITY MEASUREMENT

A. Experimental outline

To measure the directional emissivity of the PV module, a PV module is placed in the middle of the test box in a sunny day, as shown in Fig. 9. The infrared camera is placed close to the PV module to make sure the atmospheric transmission equals to 1. In this case, the temperature displayed in the infrared camera is as follows:

$$T_R^4 = \varepsilon T_0^4 + (1-\varepsilon) T_u^4. \tag{12}$$

T_R is the temperature displayed in the infrared camera, while T_0 and T_u represent the real temperature of the PV module and the environment, respectively, which are measured by thermometer. By placing the PV module in the middle of the test-box and turning the PV module in different angles while recording T_R, T_0, and T_u, the directional emissivity of different angles is calculated.

B. Experimental results of measuring directional emissivity

The infrared image taken from the experiments are displayed as in Fig. 10.

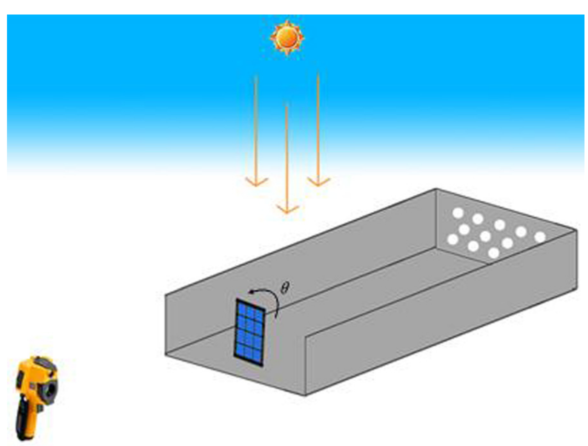

FIG. 9. Experiments to measure directional emissivity.

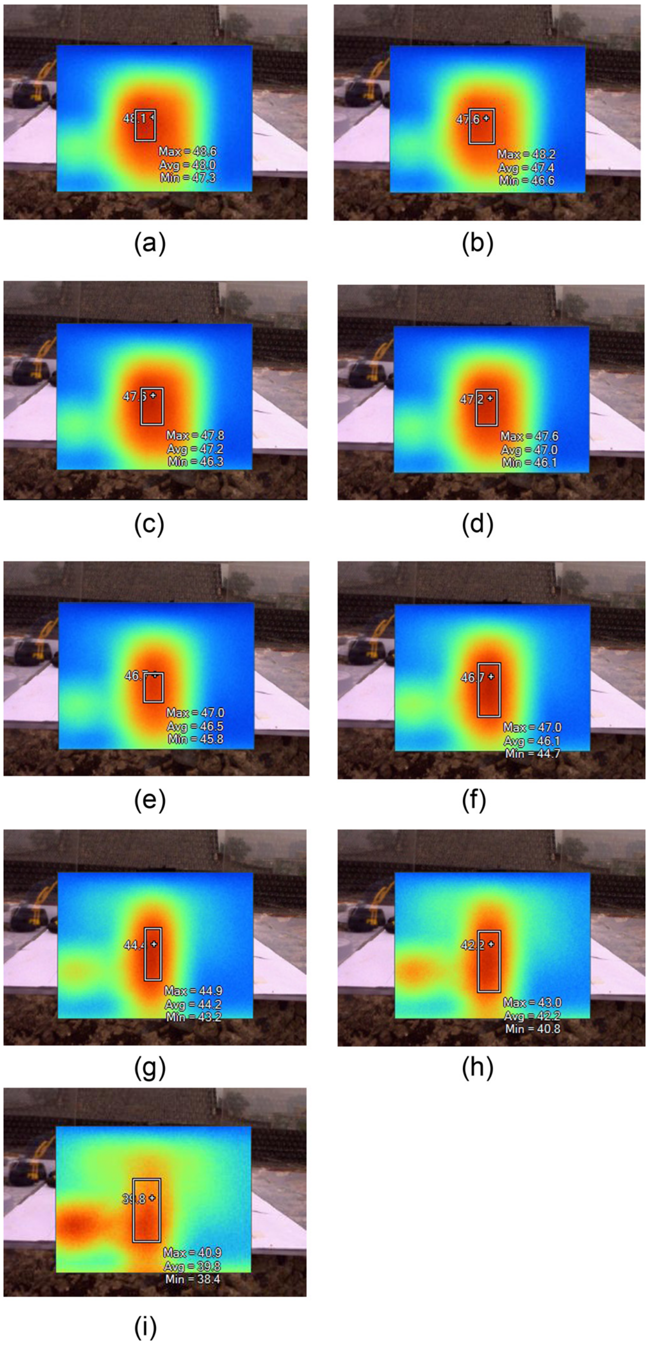

FIG. 10. Experimental results of measuring directional emissivity.

The perceived angle, as well as the T_R, T_0, and T_u for each IR image are illustrated in Table III. The average temperature of the marked out area in each IR image is selected as the T_R of the respective angle. All temperatures are transformed into Kelvin scale for calculation.

The relationship between the perceived angle and the directional emissivity is demonstrated in Fig. 11.

C. Analysis

It can be concluded from Fig. 11 that the relationship between the directional emissivity and the perceived angle is basically similar to that indicated in the work of Schmidt and Eckert,[24] that is, when θ is smaller than 60°, the directional emissivity remains relatively constant; when θ exceeds 60°, the directional emissivity drops rapidly to zero. Another phenomenon that requires attention is that when θ is smaller than 60°, ε_θ exceeds 1. This suggests that PV module is not a grey body. Temperature measurement using infrared camera cannot acquire the accurate temperature of the PV module. In order to get the accurate temperature using thermography, further research into the characteristic of the PV module is required, which is not the focus of this paper.

TABLE III. Experimental results of directional emissivity measurement.

$\theta(°)$	T_R (K)	T_0 (K)	T_u (K)	ε
0	321.15	320.15	311.15	1.116
10	320.55	320.15	310.15	1.042
20	320.35	319.15	311.15	1.157
30	320.15	318.15	309.15	1.234
40	319.65	318.15	310.15	1.196
50	319.25	318.15	310.15	1.144
60	317.35	317.15	311.15	1.034
70	315.35	317.15	312.15	0.635
80	312.95	318.15	312.15	0.130

VII. EXPERIMENTS TO MEASURE ATMOSPHERIC TRANSMISSION

In order to test whether the variation of atmospheric transmission can lead to the difference of the displayed temperature in IR image, first, experiments conducted to measure the temperature of the atmosphere as well as the temperature of the PV module at different distances, based on which the atmospheric transmission is calculated. After that the temperature is recovered and compared to that of the original image (which was taken where $\tau = 1$).

A. Atmospheric transmission calculation based on atmospheric and object temperature

The calculation method based on the atmospheric and object temperature requires the original IR image and the image taken at distance d, as well as the atmospheric temperature.

Let T_{R0} denotes the temperature in the original IR image and T_{R1} stands for the temperature in the IR image taken at distance d

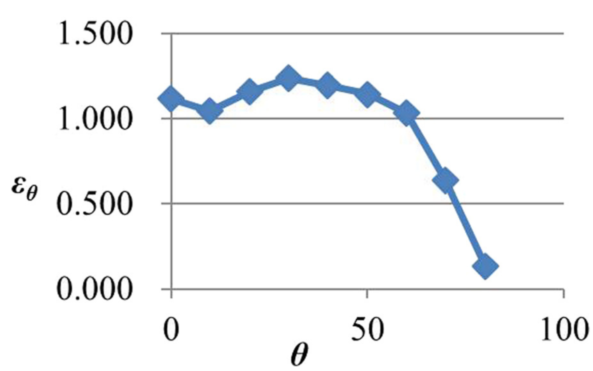

FIG. 11. Directional emissivity versus perceived angle.

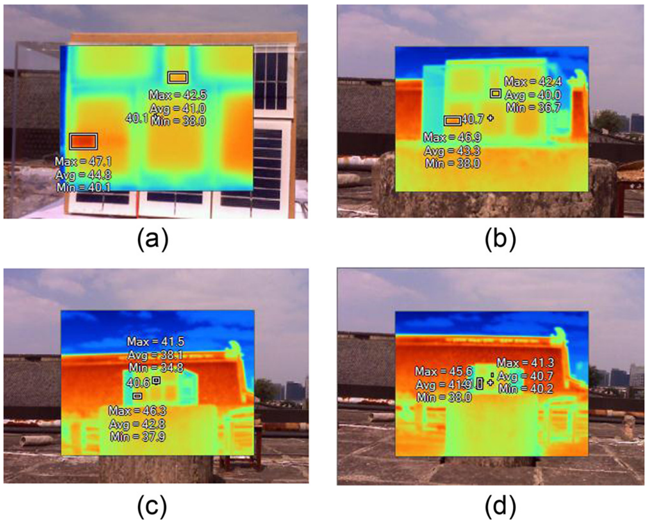

FIG. 12. Experimental results of measuring atmospheric transmission.

$$T_{R1}^4 = \tau_a T_{R0}^4 + (1-\tau_a)T_a^4. \tag{13}$$

Solving the equation yields τ_a. With the knowledge of τ_a and T_a, the original temperature of any spots in the degenerated IR image can be recovered using the following equation:

$$T_{R0} = \sqrt[4]{\frac{1}{\tau_a}[T_{R1}^4 - (1-\tau_a)T_a^4]}, \tag{14}$$

where T_{R0} is the original temperature and T_{R1} denotes the temperature displayed in the degenerated IR image.

B. Experiment to measure atmospheric transmission

Similar to the experiment of directional emissivity measurement, PV modules are placed in the test-box in this experiment. IR image are taken at the distance of 0.5 m, 1.5 m, 2.5 m, and 3.5 m. Among them, the image taken at 0.5 m is used as the original IR image, where $\tau_a = 1$. The results are demonstrated in Fig. 12. In each figure, two areas with different temperature have been marked out.

Table IV is the data retrieved from Fig. 12, as well as the calculation results of τ_a at different distance. Note that the maximum temperature of each area is used for calculation. For the calculation of τ_a, the temperature of the atmosphere as well as the object temperature is needed. The temperature of the atmosphere is 32 °C, namely, 305.15 K. The temperature of the hot area marked out in the figures is used as the object temperature.

TABLE IV. τ_a Calculation based on experimental results.

Distance (m)	Temperature of hot area (K)	Temperature of the atmosphere (K)	τ_a
0.5	320.25	305.15	1
1.5	320.05	305.15	0.980
2.5	319.45	305.15	0.938
3.5	318.75	305.15	0.889

In order to test whether it is the variation of τ_a that leads to the variation of the displayed temperature in infrared camera, the temperature of the cool area is recovered based on the calculation results of τ_a and Eq. (14). The recovered temperature is compared to the original temperature, which is the displayed temperature at 0.5 m. The results are demonstrated in Table V.

C. Analysis

From Table V, it can be concluded that at the distance of 1.5 m, the error rate after recovery increases slightly, this is because τ_a is close to 1 at this distance, and the error rate before recovery is small indeed. In this case, errors introduced from the measuring process (such as the error introduced by the thermometer, by the variation of ambient factors, etc.) can factor into the error rate after recovery. However, when the distance becomes larger, τ_a drops and the error rate after recovery is significantly reduced. This is because as τ_a drops, the error introduced by τ_a variation becomes more significant while the error introduced by the measuring process remains relatively constant. The experiment results suggest that the variation of τ_a is another major cause that leads to the gradual change phenomenon in IR image. The impact of τ_a variation can be recovered given the information of atmospheric transmission and the temperature of the ambient.

VIII. METHOD TO RETRIEVE THE REAL TEMPERATURE FROM A DEGENERATED IR IMAGE

A. Method to retrieve the real temperature from a degenerated IR image of PV modules

As explained and verified in the Secs. VI and VII, the degeneration of IR image is caused by two factors, the atmospheric transmission and directional emissivity. In order to retrieve the real temperature, it is necessary to first obtain these two parameters for the degenerated IR image. In addition, the temperature displayed on the thermal camera (T_R) as well as the temperature of the atmosphere (T_a) is needed to calculate the real temperature.

In Sec. VI, the directional emissivity has been measured (see Figure 11), which can be applied directly in the temperature retrieval process. The atmospheric transmission is reliant on the environmental factors, so it is better to measure it in the field to obtain the accurate value.

After obtaining τ_a and ε, the real temperature can be calculated as follows:

TABLE V. Recovered temperature of the cool area.

Distance (m)	T_{R1} (K)	Original temperature (K)	T_{R0} (K) recovered temperature	τ_a	Error rate before recovery	Error rate after recovery
1.5	315.55	315.65	315.75	0.980	0.235%	0.245%
2.5	314.65	315.65	315.25	0.938	2.353%	0.935%
3.5	314.45	315.65	315.56	0.889	2.824%	0.214%

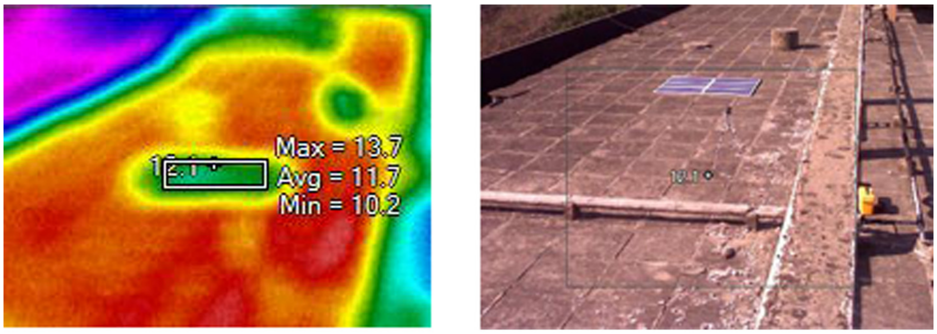

(a)   (b)

FIG. 13. (a) Degenerated IR image for temperature retrieval (Infrared view). (b) Degenerated IR image for temperature retrieval (Visible view).

$$T_0 = \sqrt[4]{\frac{\frac{[T_R^4 - (1-\tau_a)T_a^4]}{\tau_a} - (1-\varepsilon)T_a^4}{\varepsilon}}, \tag{15}$$

where T_0 is the recovered temperature.

B. Experiment to retrieve the real temperature from a degenerated IR image

The degenerated IR image is shown in Fig. 13.

The position of the thermal camera and the PV modules is displayed in Fig. 14.

According to Fig. 11, the directional emissivity at this angle is 0.445. The distance between the thermal camera and the PV module is 14.87 m.

The atmospheric transmission is measured using the method explained in Sec. VII and the results are listed in Table VI.

The result is also shown in Fig. 14 to give a clear view of how the atmospheric transmission changes.

According to the trend displayed in Fig. 14, the atmospheric transmission at the distance of 14.87 m is predicted as 0.353.

The temperature from the degenerated image is 284.85 K (see Fig. 13) and the temperature of the atmosphere is 280.15 K. According to Eq. (15), the real temperature can be calculated as 33.6 °C (306.75 K). The real temperature of the PV modules measured using thermometer is about 36 °C. The error rate is reduced from 67.5% to 6.7%. The results are displayed in Table VII.

IX. IMPACT OF THE TWO MAIN FACTORS VARIATION

A. Impact of directional emissivity variation

In order to study the impact of directional emissivity variation on the gradual change phenomenon, the directional emissivity sensitivity $S_\varepsilon^{T_R}$, which represents how the variation of ε affects the calculation result of T_R, is defined. The definition of $S_\varepsilon^{T_R}$ is as follows:

$$S_\varepsilon^{T_R} = \lim_{\Delta\varepsilon\to 0} \frac{\frac{\Delta T_R}{T_R}}{\frac{\Delta\varepsilon}{\varepsilon}} = \frac{\varepsilon}{T_R}\left(\frac{\partial T_R}{\partial \varepsilon}\right) = \frac{\varepsilon\tau_a(T_0^4 - T_u^4)}{4T_R^4}. \tag{16}$$

If $S_\varepsilon^{T_R} = 1$, it is indicated that when ε changes 10%, T_R also changes 10%.

By replacing T_R with Eq. (6), Eq. (15) can be rewritten as

$$S_\varepsilon^{T_R} = \frac{\varepsilon\tau_a(T_0^4 - T_u^4)}{4\{\tau_a[\varepsilon T_0^4 + (1-\alpha)T_u^4] + (1-\tau_a)T_a^4\}}. \tag{17}$$

$S_\varepsilon^{T_R}$ is dependent on $\varepsilon, \tau_a, T_0, T_u$, and T_a.

B. Impact of atmospheric transmission variation

Similarly, the atmospheric transmission sensitivity $S_{\tau_a}^{T_R}$ is defined to indicate how the variation of atmospheric transmission affects T_R. The definition of $S_{\tau_a}^{T_R}$ is as follows:

$$S_{\tau_a}^{T_R} = \lim_{\Delta\tau_a\to 0} \frac{\frac{\Delta T_R}{T_R}}{\frac{\Delta\tau_a}{\tau_a}} = \frac{\tau_a}{T_R}\left(\frac{\partial T_R}{\partial \tau_a}\right) = \frac{\varepsilon\tau_a(T_0^4 - T_u^4)}{4T_R^4}. \tag{18}$$

By replacing T_R with Eq. (6), Eq. (17) can be rewritten as

$$S_{\tau_a}^{T_R} = \frac{\varepsilon\tau_a(T_0^4 - T_u^4)}{4\{\tau_a[\varepsilon T_0^4 + (1-\alpha)T_u^4] + (1-\tau_a)T_a^4\}}. \tag{19}$$

The expression for $S_{\tau_a}^{T_R}$ is the same as that for $S_\varepsilon^{T_R}$.

C. Quantitative analysis of the sensitivity $S_\varepsilon^{T_R}$ and $S_{\tau_a}^{T_R}$

In order to study how ε and τ_a affect the sensitivity $S_\varepsilon^{T_R}$(or $S_{\tau_a}^{T_R}$), a MATLAB script has been programmed to plot

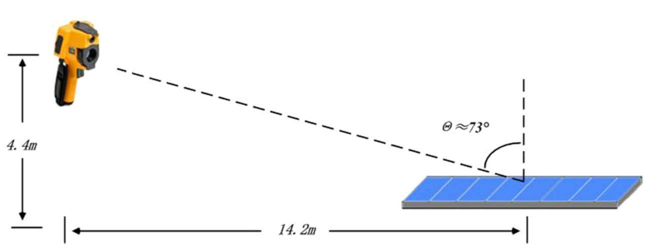

FIG. 14. Position of the thermal camera and the PV modules.

TABLE VI. Atmospheric transmission.

Distance (m)	τ_a
0.9	1
3.6	0.87
6.3	0.66
9	0.54
11.7	0.44
14.4	0.37

TABLE VII. Results of temperature recovery.

τ_a	ε	Temperature from IR image (K)	T_a(K) temperature of atmosphere	T_0(K) recovered temperature	Real temperature
0.353	0.445	284.85	280.15	306.75	309.15

the three-dimensional and two-dimensional graph based on Eq. (18), as illustrated in Fig. 13. As for the parameters, $T_0 = 320.15$ K, $T_u = T_a = 311.15$ K, which is the data from Fig. 10(a).

Note that in Fig. 13, the blue colour indicates a low value of $S_{\varepsilon}^{T_R}$ (or $S_{\tau_a}^{T_R}$), while the yellow colour indicates a higher value, and the red colour the highest. From Fig. 13, it can be concluded that when $T_0 = 320.15$ K, $T_u = T_a = 311.15$ K, the maximum value of $S_{\varepsilon}^{T_R}$(or $S_{\tau_a}^{T_R}$) is approximately 0.028. Basically, ε and τ_a have the same impact on T_R (Fig. 16). An example will help to understand such impact quantitatively. When ε remains at 1, $T_0 = 320.15$ K, $T_u = T_a = 311.15$ K, τ_a drops from 1 to 0.8 (changes 20%), T_R (the temperature displayed in the infrared camera) drops 0.56%, namely, 1.8 K. As a result, when the distance increases and τ_a drops, a gradual change phenomenon arises in the IR image. Combined with the drop of ε when $\theta < 60°$, the gradual change phenomenon becomes more significant. One way to avoid the gradual change phenomenon is to retain ε and τ_a at a low value, where the impact of both main factors become trivial, as indicated in Fig. 13. However, such method leads to other problems, which is discussed in Sec. IX D.

D. Impact of the two main factors on the difference of displayed temperature

Besides how the two main factors lead to the gradual change phenomenon, it is also necessary to study how the value of these main factors affects the difference of the displayed temperature, since it is the difference of displayed temperature that indicates the existence of defects.

Similarly, the temperature sensitivity $S_{T_0}^{T_R}$ is defined to represent how the actual temperature T_0 affects the displayed temperature T_R. The definition of $S_{T_0}^{T_R}$ is as follows:

$$S_{T_0}^{T_R} = \lim_{\Delta\tau_a \to 0} \frac{\dfrac{\Delta T_R}{T_R}}{\dfrac{\Delta T_0}{T_0}} = \frac{T_0}{T_R}\left(\frac{\partial T_R}{\partial T_0}\right) = \frac{\varepsilon \tau_a T_0^4}{T_R^4}. \tag{20}$$

By replacing T_R with Eq. (6), Eq. (19) can be rewritten as

$$S_{T_0}^{T_R} = \frac{\varepsilon \tau_a T_0^4}{\tau_a\left[\varepsilon T_0^4 + (1-\alpha)T_u^4\right] + (1-\tau_a)T_a^4}. \tag{21}$$

$S_{T_0}^{T_R}$ is also dependent on ε and τ_a, and the three-dimensional and two-dimensional graph for the relationship of $S_{T_0}^{T_R}$, ε, and τ_a are displayed in Fig. 14.

The graphs of ε, τ_a, and $S_{T_0}^{T_R}$ is similar to that of ε, τ_a, and $S_{\varepsilon}^{T_R}$ (or $S_{\tau_a}^{T_R}$), except that the maximum value of $S_{T_0}^{T_R}$ equals to 1 when $\varepsilon = \tau_a = 1$, in which case $T_0 = T_R$. The graphs for $S_{T_0}^{T_R}$ and $S_{\varepsilon}^{T_R}$ (or $S_{\tau_a}^{T_R}$) are similar because the expression for $S_{T_0}^{T_R}$ and $S_{\varepsilon}^{T_R}$ (or $S_{\tau_a}^{T_R}$) are basically the same except for a different constant factor (Fig. 17). When the value of ε and τ_a is low, the $S_{T_0}^{T_R}$ is close to 0, which means the variation of T_0 has little influence on T_R; in other words, the difference of displayed temperature becomes trivial, thus, the area with abnormal temperature is obscured. Therefore, by retaining ε and τ_a at a low value to avoid the gradual change phenomenon is impractical, otherwise the goal of defect detection is compromised. In order to offset the impact of image degeneration, the effective way is to record the value of ε and τ_a and then recover the original temperature from the degenerated IR image, which is the way introduced in Sec. VIII.

X. RESTRICTION FOR THE THERMAL CAMERA POSITION

Based on the analysis in Sec. IX, it is obvious that the position of thermal camera can affect the efficiency of monitoring. If both ε and τ_a are low, hot spots can be obscured because $S_{T_0}^{T_R}$ is close to zero (see Fig. 15). Because ε and τ_a are related to the angle and distance of between the thermal camera and the PV modules, the position of the thermal camera can affect the quality of the IR image. An IR image taken from an inappropriate position can be unrecoverable. In the first sub-section of this section, the restriction for the camera position is illustrated. After that, some rules of thumb are given to help deploy the thermal camera when monitoring PV array.

A. Restriction for the thermal camera position

In real operating condition, a hot spot in the PV modules often has a temperature difference of more than 10°. According to the experiment result in Sec. VIII, the temperature recovery method may have an error of about 3°, as the accumulation effect of the errors introduced by the measurement of other factors.

Given consideration of these errors, the position of the thermal camera should yield a temperature sensitivity higher than 0.3, so that hot spots in real operating conditions will not be obscured.

Based on this restriction and Eq. (21), the appropriate combination of ε and τ_a can be computed. For example, let $T_0 = 309.15$ K and $T_u = 280.15$ K (the real temperature and environmental temperature in Fig. 13), the appropriate combination of ε and τ_a can be computed and presented in

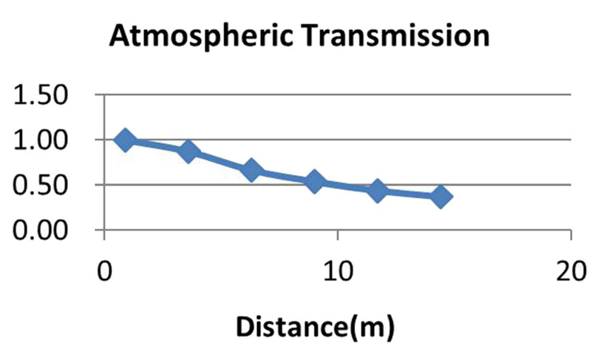

FIG. 15. Results of atmospheric transmission measurement.

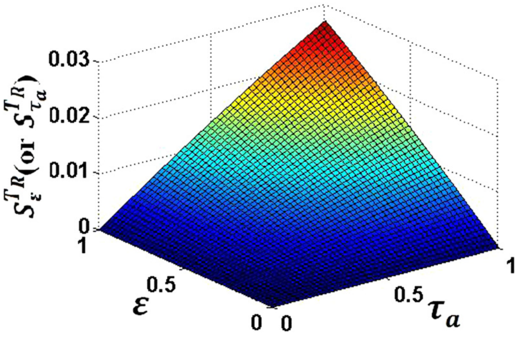

FIG. 16. Three-dimensional graph of ε, τ_a and $S_{\varepsilon}^{T_R}$(or $S_{\tau_a}^{T_R}$).

Fig. 18. The yellow area indicates the acceptable combination of ε and τ_a. By maintaining ε and τ_a in this area, the IR image will yield a temperature sensitivity higher than 0.3, and hot spots in the IR image can be recovered using the method introduced in Sec. VIII.

B. Rules of thumb for deploying thermal camera

According to the analysis in Secs. VIII and IX, the following few steps are given as the rules of thumb to quickly decide the position of the thermal camera:

(1) Acquire or estimate the following parameters: the field of view of your thermal camera ψ (available in the manual), the average temperature of the PV modules (T_0) and the atmosphere (T_a) under normal circumstance, and the area S of the PV modules.
(2) Draw the acceptable combination graph of ε and τ_a for the estimated value of T_0 and T_a.
(3) Draw an auxiliary line from the furthest side of the PV modules which forms an included angle of 60° with the ground.
(4) Find the closest spot in the auxiliary line so that the camera's field of view can cover the whole area of the PV modules on that spot. See Fig. 19.
(5) Compare ε and τ_a of the chosen spot with the graph drawn in Step 2 to decide if it is acceptable. If not, adjust the spot accordingly.

The reason to draw an auxiliary line with an included angle of 60° is because in this way the directional emissivity can be maintained at about 1, and the acceptable distance

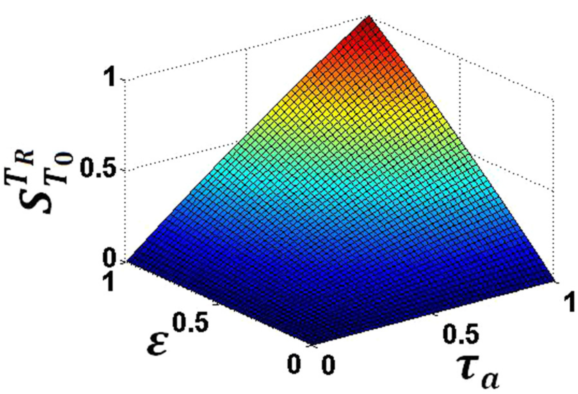

FIG. 17. Three-dimensional graph of ε, τ_a and $S_{T_0}^{T_R}$.

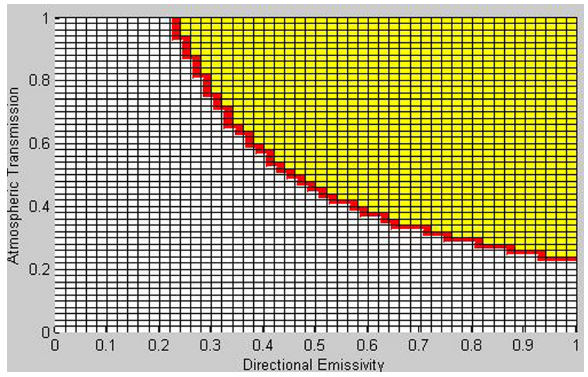

FIG. 18. Acceptable combination graph of ε and τ_a for Fig. 13.

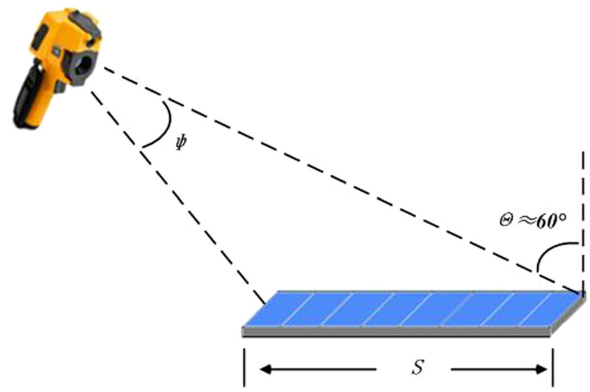

FIG. 19. Find the spot on the auxiliary line.

between thermal camera and the PV modules can be maximized.

XI. CONCLUSION

In this paper, the driver behind the IR image degeneration has been studied. Two main factors have been identified to be the cause of this phenomenon, namely, the variation of atmospheric transmission and directional emissivity. A temperature recovery method has been proposed to recover the real temperature from the degenerated image. Several conclusions can be drawn.

(1) The directional emissivity (ε_θ) of PV modules remains relatively constant when the perceived angle $\theta < 60°$; when $\theta > 60°$, ε_θ drops rapidly to zero. When monitoring a large area of PV array, the variation of θ can lead to the change of ε_θ, which is one of the causes of the IR image degeneration.
(2) As the distance increases, the atmospheric transmission (τ_a) decreases, and the displayed temperature in the infrared camera decreases. When monitoring a large area of PV array, the variation of τ_a is another cause of the IR image degeneration.
(3) When the value of τ_a and ε_θ is close to 1, the variation of τ_a and ε_θ has a larger impact on the displayed temperature. In this case, the gradual change phenomenon is more likely to happen.
(4) When the value of τ_a and ε_θ is close to 0, the temperature difference between different temperature spots becomes insignificant in the view of infrared camera.

(5) The temperature sensitivity $S_{T_0}^{T_R}$ defined in this paper can be used as the criteria to assess the quality of IR image. If $S_{T_0}^{T_R}$ is low, the hot spots in the PV modules can be obscured in the IR image.

[1]A. Zegaoui, P. Petit, M. Aillerie, J. Sawickia, and J. Charles, "Experimental validation of photovoltaic direct and reverse mode model influence of partial shading," Energy Proc. **18**, 1247–1253 (2012).
[2]A. Chouder and S. Silvestre, "Automatic supervision and fault detection of PV systems based on power losses analysis," Energy Convers. Manage. **51**, 1929–1937 (2010).
[3]M. Simon and E. Meyer, "Detection and analysis of hot-spot formation in solar cells," Sol. Energy Mater. Sol. Cells **94**, 106–113 (2010).
[4]M. Köntges, I. Kunze, S. Kajari-Schröder, X. Breitenmoser, and B. Bjørneklett, "The risk of power loss in crystalline silicon based photovoltaic modules due to micro-cracks," Sol. Energy Mater. Sol. Cells **95**(4), 1131–1137 (2011).
[5]T. Takashima, J. Yamaguchi, K. Otani, T. I. Oozeki, K. Kato, and M. Ishida, "Experimental studies of fault location in PV module strings," Sol. Energy Mater. Sol. Cells **93**(6–7), 1079–1082 (2009).
[6]Y.-H. Liu, S.-C. Huang, J.-W. Huang, and W.-C. Liang, "A particle swarm optimization-based maximum power point tracking algorithm for PV systems operating under partially shaded conditions," IEEE Trans. Energy Convers. **27**(4), 1027–1035 (2012).
[7]K. Ishaque, Z. Salam, and A. Syafaruddin, "A comprehensive MATLAB Simulink PV system simulator with partial shading capability based on two-diode model," Sol. Energy **85**(9), 2217–2227 (2011).
[8]J. Kurnik, M. Jankovec, K. Brecl, and M. Topic, "Outdoor testing of PV module temperature and performance under different mounting and operational conditions," Sol. Energy Mater. Sol. Cells **95**(1), 373–376 (2011).
[9]O. Breitenstein, J. P. Rakotoniaina, M. H. Al Rifai, and M. Werner, "Shunt types in crystalline silicon solar cells," Prog. Photovoltaics **12**(7), 529–538 (2004).
[10]C. Meola, "A new approach for estimation of defects detection with infrared thermography," Mater. Lett. **61**(3), 747–750 (2007).
[11]N. Gokmen, E. Karatepea, B. Celika, and S. Silvestre, "Simple diagnostic approach for determining of faulted PV modules in string based PV arrays," Sol. Energy **86**(11), 3364–3377 (2012).
[12]Cl. Buerhopa, D. Schlegela, M. Niessb, C. Vodermayerb, R. Weißmanna, and C. J. Brabeca, "Reliability of IR-imaging of PV-plants under operating conditions," Sol. Energy Mater. Sol. Cells **107**, 154–164 (2012).
[13]A. Krenzinger and A. C. Andrade, "Accurate outdoor glass thermographic thermometry applied to solar energy devices," Sol. Energy **81**, 1025–1034 (2007).
[14]T. Trupke, R. A. Bardos, M. C. Schubert, and W. Warta, "Photoluminescence imaging of silicon wafers," Appl. Phys. Lett. **89**, 044107 (2006).
[15]Y. Hu, B. Gao, X. Song, G. Y. Tian, K. Li, and X. He, "Photovoltaic fault detection using a parameter based model," Sol. Energy **96**, 96–102 (2013).
[16]Y. Hu, H. Chen, R. Xu, D. Yu, and R. Li, "Maximum power point tracking under shadowed conditions," Proc. Chin. Soc. Electr. Eng. **32**(9), 10–20 (2012).
[17]H. Patel and V. Agarwal, "Matlab—based modeling to study the effects of partial shading on PV array characteristics," IEEE Trans. Energy Convers. **23**(1), 302–310 (2008).
[18]A. Luque, G. Sala, and J. C. Arboiro, "Electric and thermal model for non-uniformly illuminated concentration cells," Sol. Energy Mater. Sol. Cells **51**, 269–290 (1998).
[19]H. F. Tsai and H. L. Tsai, "Implementation and verification of integrated thermal and electrical models for commercial PV modules," Sol. Energy **86**(1), 654–665 (2012).
[20]J. A. Tsanakas and P. N. Botsaris, "Passive and active thermographic assessment as a tool for condition-based performance monitoring of photovoltaic modules," J. Sol. Energy Eng. **133**(2), 021012 (2011).
[21]M. Usama Siddiqui, A. F. M. Arif, L. Kelley, and S. Dubowsky, "Three-dimensional thermal modeling of a photovoltaic module under varying conditions," Sol. Energy **86**(9), 2620–2631 (2012).
[22]A. D. Jones and C. P. Underwood, "A thermal model for photovoltaic systems," Sol. Energy **70**(4), 349–359 (2001).
[23]T. Inagaki and O. Yoshizo, "Surface temperature measurement near ambient conditions using infrared radiometers with different detection wavelength bands by applying a grey-body approximation: estimation of radiative properties for non-metal surfaces," NDT&E Int. **29**(6), 363–369 (1996).
[24]E. Schmidt and E. Eckert, "Über die Richtungsverteilung der Wärmestrahlung von Oberflächen," Forschung Im Ingenieurwesen **6**(4), 175–183 (1935).